Chapter 11

Numerical Modelling of the Seismic Behaviour of Gravity-Type Quay Walls

Babak Ebrahimian

Additional information is available at the end of the chapter

http://dx.doi.org/10.5772/55027

1. Introduction

Gravity quay walls are the most common type of construction for docks and harbours because of their durability, ease of construction and capacity to reach deep seabed levels. Gravity quay walls are designed for three main criteria; sliding, overturning and allowable bearing stress under the base of quay wall. Although the design of gravity quay walls has been reasonably well understood for static loads, but analysis under seismic loads is still in being developed. During strong ground shaking, the pore water pressure of cohesionless saturated backfill soils builds up. This pressure increase not only causes the lateral forces on the wall (which leads to wall failure), but also reduces the effective stress of backfill soil which may result in liquefaction. The occurrence of liquefaction in backfill soil was the main reason of damages from past earthquakes to gravity quay walls (e.g., in 1964 at Nigata Port (Hayashi et al. 1966), in 1993 at Kushiro-oki, and in 1994 at Hokkaido Toho-oki (Sasajima et al. 2003)). Moreover, observations of 24 marine structures in 1999 earthquake at Kocaeli, Turkey showed the seaward movement of quay walls due to the liquefaction of backfill soils (Sumer et al. 2002). The same observations were reported in 1999 during the Chi Chi earthquake in Taiwan (Chen and Hwang 1999).

The seismic coefficient method containing Mononobe-Okabe's formula is usually used in the design of gravity-type quay walls to resist earthquake damages but this design method does not take into account the liquefaction of backfill soil and its associated deformations (Sasajima, et al. 2003). Furthermore, conventional design method of quay walls is based on providing capacity to resist a design seismic force, but it does not provide information on the performance of a structure when the limit of the force-balance is exceeded. In this regard, gravity quay walls failures have caused much progress in the development of deformation-based design methods for waterfront structures. Accordingly, much significant experimental and theoretical research works have been done (Sugano et al. 1996; Inagaki et al. 1996; Iai 1998; Iai et al. 1998; Iai and

Sugano 2000; Ichii et al. 2000; Inoue et al. 2003; Nozu et al. 2004; Mostafavi Moghadam et al. 2009 and 2011). A new design methodology, named performance-based design, has born from lessons learned caused by earthquakes in 1990's to overcome the limitations of conventional seismic design (PIANC 2001). In this framework, lateral spreading of the saturated backfill and foundation soils along with the effect of quay wall as the supporting structure (saturated soil-structure interaction) are taken into account as a more logical design.

Predicting the response of a structure retained a liquefiable soil during an earthquake is highly dependent on adequately accounting for the effects of pore water pressure development, stress-strain softening and strength reduction in the soil on the system behavior. Thus, it is required to perform dynamic analyses that account for the saturated soil-structure interaction effects using numerical modeling techniques. Several researchers have reported the use of numerical analysis for predicting the behavior of liquefiable soil measured in laboratory tests or field case histories. Iai et al. (1998) reported that FLIP code can successfully predict the seismic behavior of port structures. Yang and Parra developed CYCLIC code and reported successful predictions of the seismic behavior of gravity quay wall placed on liquefiable sand and calibrated the numerical results with centrifuge tests (Parra 1996; Yang 2000). Both the codes DYSAC2 and DYNAFLOW are reported by Arulanandan (1996) as having adequately predicted the response of a submerged embankment subjected to dynamic loading in a centrifuge test. According to Madabhushi and Zeng (1998), the code SWANDYNE successfully predicted the seismic response of a gravity quay wall rested on liquefiable sand modeled in the centrifuge. Finn reported the successful validation of TARA-3 using centrifuge tests results (Finn et al. 1991). The successful use of FLAC package for prediction of the behavior of caisson retaining walls in liquefiable soils was reported by Dickenson and Yang (1998). They used a nonlinear effective stress analysis method based on the Mohr-Coulomb constitutive model and a pore water pressure increment scheme based on the work of Seed and his co-workers (e.g. Martin et al. 1975; Seed and DeAlba 1986). Likewise, McCullough and Dickenson, who used the same analysis method and soil model in FLAC, reported fairly good agreement between predicted and measured permanent horizontal displacements at top of five anchored sheet pile bulkhead walls in liquefiable soils subjected to different earthquakes in Japan between 1987 and 1993 (McCullough and Dickenson 1998). It should be noted that the assumption of the Yang and McCullough was that the foundation soil is non-liquefiable. A hyperbolic type stress-strain formulation developed by Pyke (1979) along with the pore water pressure build up model proposed by Byrne (1991) was implemented in FLAC code by Cooke (2001). They concluded that Pyke-Byrne model over-predicts the horizontal displacement of gravity quay walls modelled in centrifuge within a factor of approximately two.

Recently, Ebrahimian et al. (2009) have carried out a series of two dimensional fully coupled effective stress dynamic analyses in order to study the deformation of quay walls and the liquefaction potential of backfill soils. Additionally, several 1g shaking table tests have been executed to verify the obtained numerical results. They showed based on the lessons learned obtained from numerical results, a safer design of gravity-type quay walls can be developed. Correspondingly, Mostafavi Moghadam et al. (2009) conducted finite difference effective-stress analyses to investigate the seismic performance of caisson quay walls. Their obtained

http://dx.doi.org/10.5772/55027

numerical results in terms of seaward movement, settlement and inclination of wall as well as the total pressure recorded behind the caisson wall were compared with 1g shaking table tests results. It was demonstrated that the numerical results appropriately supports the experimental results obtained by model tests.

In this chapter, firstly some aspects related to calibration of a numerical model are discussed. Then, the numerical results are verified by comparing the calculated values with corresponding ones obtained from 1g shaking table tests. A series of two dimensional fully coupled effective stress dynamic analyses are carried out in order to study the deformation of quay wall, liquefaction potential and failure mechanisms of soil-wall system during seismic loading. The Finn and Byrne model Byrne (1991) is used with some minor modifications to model pore pressure build up during seismic loading. Afterwards, computational parametric studies are performed to investigate the effects of backfill soil properties and input excitation characteristics on the seismic behaviour of gravity-type quay walls including the residual deformation of wall, liquefaction potential and failure modes of soil-wall system.

Several 1g shaking table tests have been executed to verify the obtained numerical results. It is found that the extent of liquefaction and the deformation pattern of soil-wall system that includes seaward displacement, tilting and settlement (as typical failure modes of quay walls due to earthquake) resulted from numerical analyses agree reasonably well with the actual observations in shaking table tests. During seismic excitation, no evidence of liquefaction has detected near the quay wall but liquefaction occurs at some landward distance from the wall. Based on the current results, it seems possible to develop a safer design of gravity-type quay walls by using lessons learned from the present numerical analyses.

2. Description of the numerical method

In this research, a two-dimensional (2D) reference model is developed to simulate the seismic performance of gravity-type quay walls in a rational way. Nonlinear time history dynamic analysis is conducted using computer program FLAC 2D (Itasca 2004). FLAC 2D is an explicit finite difference program for modeling soil-structure interaction analysis under static and seismic loading conditions. Here, numerical approach is based on a continuum finite difference discretization applying Lagrangian approach (Itasca 2004). Every derivative in the set of governing equations is directly replaced by algebraic expression written in terms of field variables (e.g., stress or displacement) at discrete point in space. Regarding dynamic analysis, explicit finite difference scheme is applied to solve the full equation of motion using the lumped grid point masses derived from the real density of surrounding zone. The calculation sequence first invokes the equations of motion for deriving new velocities and displacements from stresses and forces; then, strain rates are derived from velocities, and new stresses from strain rates. Every cycle around the loop corresponds to one time step. Each box updates all grid variables from known values which are fixed over the time step being executed (Figure 1).

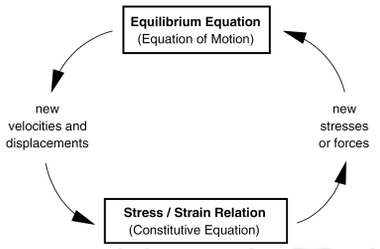

Figure 1. Basic explicit calculation cycle (Itasca 2004)

The equation of motion, in the simplest form, relates the acceleration ($d\dot{u}/dt$) of a mass (m) to the applied force (F) which may vary with time. Newton's law of motion for the mass-spring system is:

$$m\frac{d\dot{u}}{dt} = F \tag{1}$$

In a continuous solid body, Eq. (1) is generalized as follows:

$$\rho\frac{\partial\dot{u}_i}{\partial t} = \frac{\partial\sigma_{ij}}{\partial x_j} + \rho g_i \tag{2}$$

where, ρ = mass density; t = time; x_j = components of coordinate vector; g_i = components of gravitational acceleration (body forces); σ_{ij} = components of stress tensor; i = components in a Cartesian coordinate frame.

For problem analysis, the strain rate tensor and rotation rate tensor, having the velocity gradients, are calculated by the following equations:

$$e_{ij} = \frac{1}{2}\left[\frac{\partial\dot{u}_i}{\partial x_j} + \frac{\partial\dot{u}_j}{\partial x_i}\right] \tag{3}$$

$$\omega_{ij} = \frac{1}{2}\left[\frac{\partial\dot{u}_i}{\partial x_j} - \frac{\partial\dot{u}_j}{\partial x_i}\right] \tag{4}$$

where, e_{ij}= components of strain rate; ω_{ij}= components of rotation rate; $\dot{u}_i$= components of velocity.

The specific mechanical relationship is used in order to obtain the stress tensor as below:

http://dx.doi.org/10.5772/55027

$$\sigma_{ij} = M\left(\sigma_{ij}, \dot{e}_{ij}, \kappa\right) \tag{5}$$

where, M = specific rule of behaviour; κ= history parameters (based on the specific rules which may or may not exist).

2.1. Modeling procedure

Firstly, a static analysis considering the effect of gravity with the Mohr-Coulomb elastic perfectly plastic constitutive soil model is performed to establish the in-situ stresses before seismic loading. The water within the soil is modeled directly, and is allowed to flow during the static solutions. Static solutions are obtained by including damping terms that gradually remove kinetic energy from the system. Then, boundary pressures equivalent to fluid weight is applied along the bottom of the sea and the front side of the caisson. Once initial stress state is established in the model and the soil model is changed to a pore pressure generation constitutive model, the effective stress dynamic analysis is started. For dynamic analysis, the acceleration record is applied to the nodes along the bottom of numerical grid. During the dynamic solutions excess pore water pressures are allowed to generate and also the dissipation of these pore pressures is modelled. To this end, the Finn and Byrne model (Finn et al. 1977; Byrne 1991) is modified and used to carry out coupled dynamic groundwater flow calculations. This effective stress analysis which take into account the effects of seismically induced pore water pressures is used to investigate the degree and extend of liquefaction that occur in backfill. It should be noted that, all analyses are performed under fully drained condition. One key advantage of the coupled numerical approach is the ability to account for the interdependent effects of various mechanisms and phenomena on each other as the numerical computations proceed. For instance, when an effective stress formulation is used, the inclusion of pore water pressure generation in the simulation can impact the strength and stress-strain behavior of the soil during shaking in the same manner as in the field. For the sake of simplicity in defining the performance of a quay wall during an earthquake, the author has focused on the horizontal movement because most of the gravity-type quay walls exhibited a failure pattern predominantly in the form of excessive horizontal movement rather than other damages. The numerical grid for a typical quay wall and foundation soil used in the current study is illustrated in Figure 2. Numerical model represents a backfill of constant depth retained by quay wall rested on a very dense foundation.

2.2. Soil constitutive model

In static analysis, the Mohr-Coulomb constitutive model is used to model the behaviour of sandy soil. The linear behaviour is defined by elastic shear and drained bulk modulus. The shear modulus of sandy soil is calculated with the formula given by Seed and Idriss (1970):

$$G_{\max} = 1000\, k_{2\max} \left(\sigma'_m\right)^{0.5} \tag{6}$$

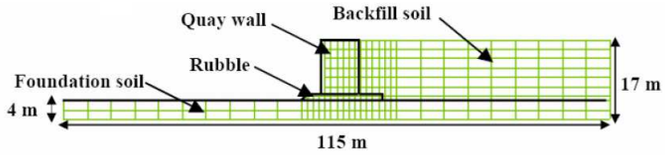

Figure 2. Numerical grid constructed in FLAC

where, G_{max} is the maximum (small strain) shear modulus in pounds per square foot, psf (it is later converted to kPa to be consistent with metric units being used), k_{2max} is the shear modulus number (Seed and Idriss 1970), and σ'_m is the mean effective confining stress in psf. The Poisson's ratio is taken as 0.35.

For pore water generation during dynamic analysis, the updated model proposed by Byrne (1991) is incorporated to account the development of pore water pressure build up as an effect of volumetric strain induced by the cyclic shear strain using the following formulation:

$$\Delta\varepsilon_v = C_1 \exp\left(C_2\, \varepsilon_v / \gamma\right) \tag{7}$$

where, $\Delta\varepsilon_v$ is the volumetric strain increment that occurs over the current cycle, ε_v is the accumulated volumetric strain for previous cycle, γ is the shear strain amplitude for the current cycle, and C_1 and C_2 are constants dependent on the volumetric strain behavior of sand. According to Byrne (1991), the constant C_1 in equation 7 controls the amount of volumetric strain increment and C_2 controls the shape of volumetric strain curve. These constants are estimated using:

$$C_1 = 7600\left(Dr\right)^{-2.5} \tag{8}$$

$$C_2 = 0.4/C_1 \tag{9}$$

where, Dr is the relative density of soil in percent. To provide constitutive model that can better fit the curves of shear modulus reduction and damping ratio derived from the experimental tests data, two different modifications to soil model are implemented as a part of this research to assess the potential for predicting liquefaction phenomenon and associated deformations. To represent the nonlinear stress-strain behavior of soil more accurately that follows the actual stress-strain path during cyclic loading, the masing behavior is implemented into FLAC which works with Byrne model by a FISH subroutine as a first modification.

Since, there is a need to accept directly the same degradation curves derived from the test data in fully nonlinear method to model the correct physics, the second modification is related to incorporate such cyclic data into a hysteretic damping model for FLAC.

http://dx.doi.org/10.5772/55027

Modulus degradation curves imply a nonlinear stress-strain curve. An incremental constitutive relation can be derived from the degradation curve, described by $\tau/\gamma = M_s$, where τ is the normalized shear stress, γ is the shear strain and M_s is the normalized secant modulus. The normalized tangent modulus, M_t, is descried as

$$M_t = d\tau / d\gamma = M_s + \gamma . dM_s / d\gamma \tag{10}$$

The incremental shear modulus in a nonlinear simulation is then given by GM_t, where G is the small-strain shear modulus of the material.

2.3. Full non-linear dynamic analysis

Equivalent linear analysis is the common method used for evaluating the seismic behaviour of earth structures. In this approach, first, the responses are linearly analyzed using the initial values of damping ratio and shear modulus. Then, the new values of damping ratio and shear modulus are estimated, using maximum value of shear strain and laboratory curves. These values are used for redoing the analysis. This procedure is repeated several times until the material properties show no variation. Therefore, no non-linear effect is directly captured by this method as it assumes linearity during the solution process. Strain-dependent modulus and damping functions are considered roughly in order to approximate some effects of non-linearity (damping and material softening).

In the non-linear analysis, employed in this study, the non-linear stress-strain relationship is directly followed by each zone. Damping ratio and shear modulus of the materials are calculated automatically at different strain levels. The real behaviour of soil, under cyclic loading, is non-linear and hysteretic. Such behaviour can be simulated by Masing model (Masing 1926), which can model the dynamic behaviour of soil. In this model, the shear behaviour of soil may be explained by a backbone curve as:

$$F_{bb}(\gamma) = \frac{G_{\max}\gamma}{1 + \left(G_{\max}/\tau_{\max}\right)|\gamma|} \tag{11}$$

where, $F_{bb(\gamma)}$ = backbone or skeleton function; γ= shear strain amplitude; G_{max} = initial shear modulus; τ_{max} = maximum shear stress amplitude.

Stress-strain curve follows the backbone curve in the first loading, as shown in Figure 3(a); however, for explaining the unload-reload process, the above equation should be modified. If load reversal occurs at the point (τ_r, γ_r), stress-strain curve follows the path given by the below formula:

$$\frac{\tau - \tau_r}{2} = F_{bb}\left[\frac{\gamma - \gamma_r}{2}\right] \tag{12}$$

In other words, the shapes of unload-reload curves are similar to that of backbone curve (with the origin shifted to the loading reversal point) except they are enlarged by a factor of 2, as shown in Figure 3(b). The Equations (9) and (10) describe the Masing behaviour (Masing 1926).

Masing rules seem not to be enough for precise explanation of soil response under general cyclic loading. Finn et al. (1977) developed modified rules to describe the irregular loading. They suggested that unloading and reloading curves follow the concerning two rules. If the new unloading or reloading curve exceeds the last maximum strain and cut the backbone curve, it will follow the backbone curve up to meeting the next returning point, as shown in Figure 3(c). If a new unloading or reloading curve passes through the previous one, it will follow the former stress-strain curve, as shown in Figure 3(d). According to this model, the tangent shear modulus can be defined at the points on the backbone and new reloading-unloading curves by the Formulas (11) and (12), respectively, as:

$$G_t = G_{\max} \Bigg/ \left[1 + \frac{G_{\max} |\gamma|}{\tau_{\max}} \right]^2 \tag{13}$$

$$G_t = G_{\max} \Bigg/ \left[1 + \frac{G_{\max}}{2\tau_{\max}} |\gamma - \gamma_r| \right]^2 \tag{14}$$

Based on the results, obtained in this research, the shear stress decreases as the number of load cycles increases; it means that shear stress-strain curves are more inclined. In this study, Masing rules are implemented into FLAC via a series of FISH functions in order to simulate the non-linear stress-strain relationships.

2.4. Material properties and input seismic loading

For the gravity quay wall, the concrete caisson is modeled by linear elastic elements. The granular backfill is modeled as a purely frictional, elastic–plastic soil with a Mohr–Coulomb failure criterion. Strength properties for sandy soil at relative densities of 25 and 85 percent are obtained based on correlations in literature. Maximum shear moduli (i.e. modulus at a strain level of approximately 0.0001%) for Sandy soil are determined from formula developed by Seed and Idriss (1970), given in Equation (6). Hydraulic conductivities are derived from constant head permeability tests. Values for the constants C_1 and C_2 used in the volumetric strain equation (Equation (7)) are obtained from Equations 8 and 9. The material properties of soil layers are listed in Table 1.

After static equilibrium is achieved (end of static construction stage), the full width of the foundation is subjected to the variable-amplitude harmonic ground motion record illustrated in Figure 4. The mathematical expression for input acceleration is given by:

$$\ddot{U}(t) = \sqrt{\beta \, \mathrm{e}^{-\alpha t} \, t^{\eta}} \, \sin(2\pi f t) \tag{15}$$

http://dx.doi.org/10.5772/55027

where, α=3.3, β=1.3 and η=10 are constant coefficients, f is the base acceleration frequency and t is the time.

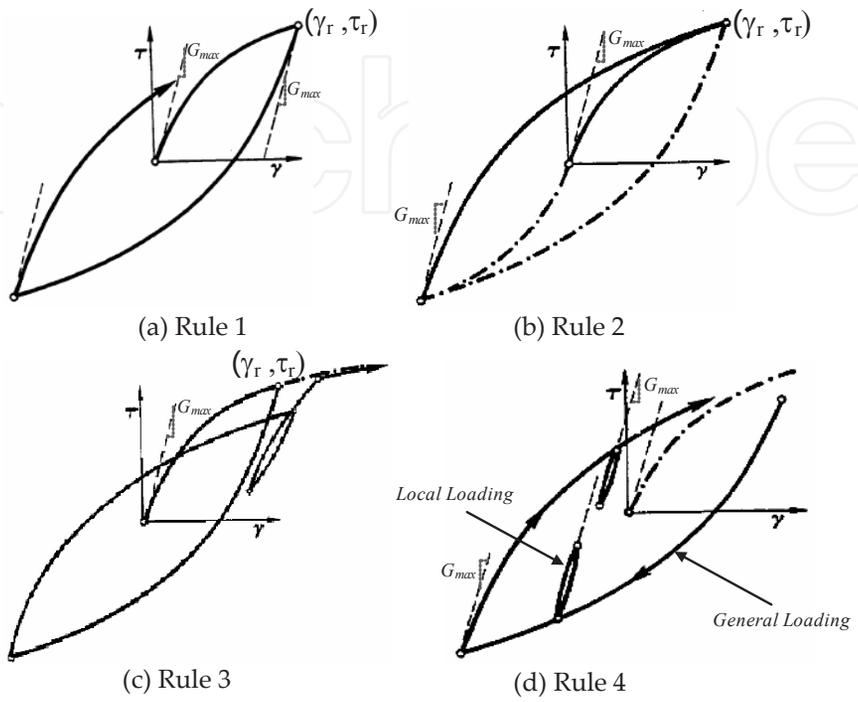

Figure 3. General patterns of loading, unloading and reloading paths in Masing model

	γ_d	G	K	Friction	C_1	C_2
	(kN/m³)	*(MPa)*	*(MPa)*	*(degree)*		
Caisson quay wall	2400	83.33	111.11	-	-	-
Backfill soil	1520	35	75.83	25	2.432	0.164
Foundation soil	1600	130	281.66	38	0.114	3.508
Rubble foundation	1800	155	206.66	40	-	-

Table 1. Soil properties

2.5. Structural properties

The structural element consists of a gravity quay wall supported on very dense foundation soil. The structural element is modeled within FLAC as elastic element. The soil-structure interaction between soil and wall including normal and shear springs. The FLAC manual (Itasca 2004) recommends as a rule of thumb that k_s and k_n be set to ten times the equivalent stiffness of the stiffest neighboring zone (see equation (16) below).

$$k_n = k_s = 10 \times \max\left[\frac{\left(K + \frac{4}{3}G\right)}{\Delta Z_{\min}}\right] \tag{16}$$

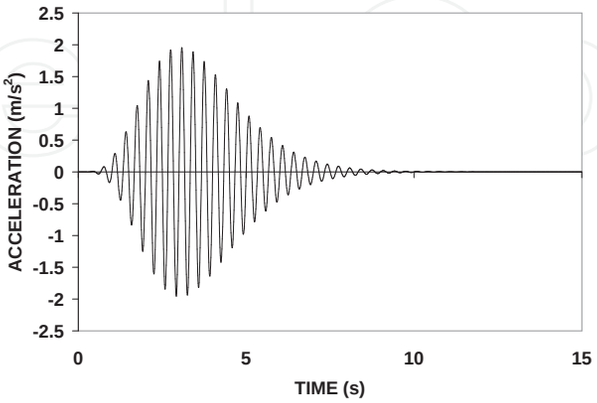

Figure 4. Seismic excitation applied to the bottom of numerical model

where K and G are the bulk and shear moduli; and $\Delta z_{\min}$ is the smallest width of an adjoining zone. The max [ ] notation indicates the maximum value over all zones adjacent to the interface.

In the case of a rough wall, modelling the interface between the soil and the wall is invariably an integral part of the analysis. In the case of soil–structure interaction, the interface is considered stiff compared to the surrounding soil, but it can slip and open in response to the loading. Joints with zero thickness are more suitable for simulating the frictional behaviour at the interface between the wall and the soil. The interface model is described by Coulomb law (Itasca 2004) to simulate the soil/wall contact. The interface element properties are summarized in Table 2.

Surface	k_n	k_s	Friction
	(Pa/m)	*(Pa/m)*	*(degree)*
Quay wall with rubble	$1e^{11}$	$1e^{11}$	20
Quay wall with backfill soil	$1e^{11}$	$1e^{11}$	12

Table 2. Interface element properties

2.6. Fluid properties

The modeled fluid is representative of seawater with a unit weight of 1027 kg/m^3 and a bulk modulus of 2 GPa. An estimated pore pressure distribution is initialized in the model prior to the initial static stress state solution.

http://dx.doi.org/10.5772/55027

2.7. Hydrodynamic effects

Based on Westergaard's approach (1931), effects of hydrodynamic pressure can be approximately considered as added masses acting with the quay wall. The added mass increases parabolically with depth and is defined by

$$m(y) = \frac{7}{8} M_W \sqrt{h.y} \tag{17}$$

Where m(y) is the variation of mass with depth y. M_w is the mass density of water and h is the overall depth of the water in front of the quay wall. The added mass can be reasonably modeled as a simple-supported beam element which possess the corresponding mass m(y) and is free to move in the horizontal direction.

The water in front of the wall is modeled indirectly by including the resulting water pressures along the boundaries. This allows a simple modeling of the water, but does not account for the dynamic interaction of the wall and water.

2.8. Boundary conditions

Many geotechnical problems can be idealized by assuming that the regions remote from the area of interest extend to infinity. As the capability of computer is limited, the unbounded theoretical models have to be truncated to a manageable size by using artificial boundaries. In practice, the numerical model for the quay wall system should be extended to a sufficient depth below the ground level and to a sufficient width to consider local site effects and soil-structure interaction. During the static analysis, the bottom boundary is fixed in the both horizontal and vertical directions and the lateral boundaries are just fixed in the horizontal direction. In dynamic problems fixed boundary condition will cause the reflection of outward propagating waves back into the model.

Thus, absorbing boundaries proposed by Lysmer and Kuhlemeyer (1969) are applied to the lateral boundaries in the model during dynamic analyses. It is based on the use of independent dashpots in the normal and shear directions at the lateral boundaries.

2.9. Damping

Material damping in a soil is generally caused by its viscous properties, friction and the development of plasticity. Indeed, the role of the damping in the numerical models is to reproduce in magnitude and form the energy losses in the natural system when subject to a dynamic load. The dynamic damping in the model is provided by the Rayleigh damping option provided in FLAC. A damping percentage of 5 percent is used which is a typical value for geologic materials (Itasca 2004). The damping frequency is chosen by examining the undamped behavior of the numerical model. A damped frequency of 1 Hz is used for the present model. In each dynamic analysis, 5 percent Rayleigh damping is included for the soil elements in addition to the hysteretic damping already incorporated in the nonlinear stress-strain model.

2.10. Element size

To avoid the numerical distortion of the propagating wave in dynamic analysis the spatial element size, ΔL, must be smaller than approximately one-tenth to one-eighth of the wavelength associated with the highest frequency component of the input wave (Kuhlemeyer and Lysmer 1973):

$$\Delta L = \lambda / 9 \tag{18}$$

In general, the cut-off frequency for geotechnical earthquake engineering problems should be no less than 10 Hz (ASCE 2000). Considering above criteria, element size is defined small enough to allow seismic wave propagation throughout the analysis. A finer mesh is used in sensitive areas such as below and near quay wall. A coarser mesh has been chosen for other areas in order to save computer analysis time.

2.11. Time step

To complete the numerical solution, it is necessary to integrate the governing equations in time in an incremental manner. The time step of the solution should be sufficiently small to accurately define the applied dynamic loads and to ensure stability and convergence of the solution. In the current FLAC model, the time step is approximately 10^{-6} second.

The convergence criterion for FLAC is the ratio defined to be the maximum unbalanced force magnitude for all the gridpoints in the model divided by the average applied force magnitude for all the gridpoints.

3. Verification

To validate the implementation of the masing rule and hysteresis damping in FLAC program, the simulation of one-zone sample with modified Byrne model is done by using the unit cell as shown in Figure 5 incorporated with the implemented rules.

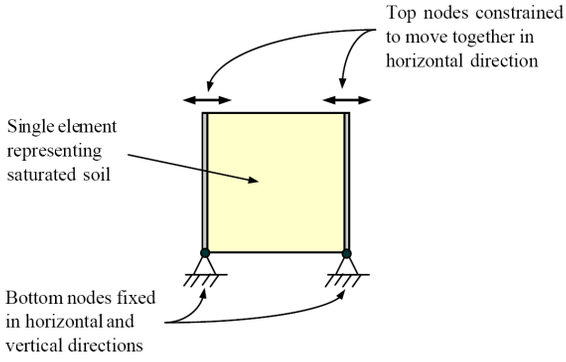

Figure 5. One-zone model in FLAC for simulating cyclic simple shear test

http://dx.doi.org/10.5772/55027

The one-zone sample is modeled with FLAC that this consist of a sandy soil which is given a periodic motion at its base. Vertical loading is by gravity only. Equilibrium stresses and pore pressures are installed in the soil, and pore pressure and effective stress (mean total stress minus the pore pressure) are established within the soil. The modified Byrne model is applied for the soil. The results based on Equation (7) are shown in Figures 6 and 7.

Figure 6 indicates the pore pressure build up in a single zone. It can be seen that the effective stress reaches zero after about 20 cycles of shaking (2 seconds, at 5 Hz). At this point, liquefaction can be said to occur. This test is strain-controlled in the shear direction. The stress/strain loops for the one-zone sample for several cycles are shown in Figure 7. It can be observed that shear modulus decreases with increasing shear strain. The hysteretic model seems to handle multiple nested loops in a reasonable manner. There is clearly energy dissipation and shear stiffness degradation during seismic loading. Due to the satisfactory modeling of the validation case, the numerical model is used to perform parametric studies on caisson quay wall, as described in the pervious sections.

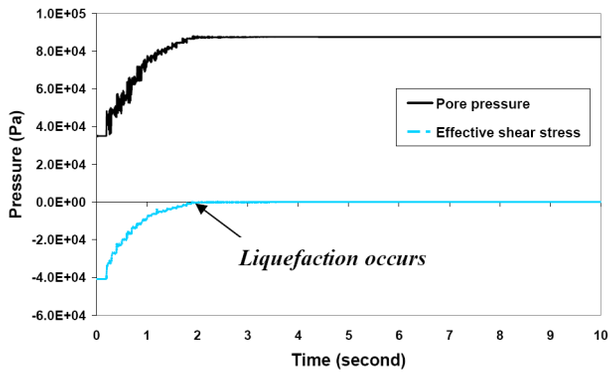

Figure 6. Pore pressure generation and effective stress time histories during seismic loading

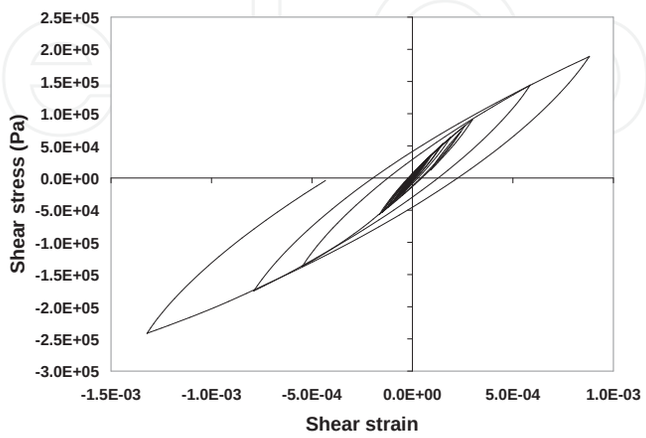

Figure 7. Hyteresis loop in a one-zone sample element

A series of 1g shaking table tests have been executed in order to verify the obtained numerical results. It is attempt to create almost similar conditions between laboratory model test and numerical model. The liquefiable soil is modeled by loose sand and non-liquefiable soil is modeled by very dense sand. The seismic excitation is shown in Figure 8. The numerical results are presented and compared to those of corresponding shaking table test. Figure 9(a) shows the permanent deformation pattern of the numerical model after dynamic excitation. The nodal displacement vectors are presented in Figure 9(b). As may be expected, more ground surface settlement is observed in the backfill near the wall than at far field. A rigid body rotation of the wall (tilt) to the seaward direction is also clearly seen. The deformation pattern of model test at the end of seismic loading is presented in Figure 10. The trend of deformation behind quay wall and movement of the wall are in fairly good agreement with numerical results. Comparisons between the calculated and measured results (Calculated: numerical and Measured: experimental results) are made in Figure 11.

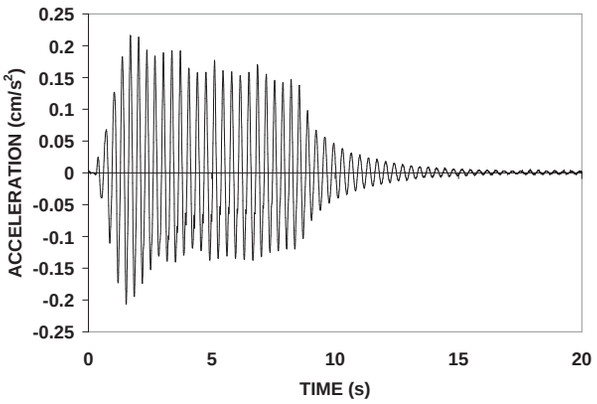

Figure 8. Input base excitation

Figure 9. Computed post-earthquake (a) deformed shape, (b) nodal displacement vectors for the quay wal after the seismic loading

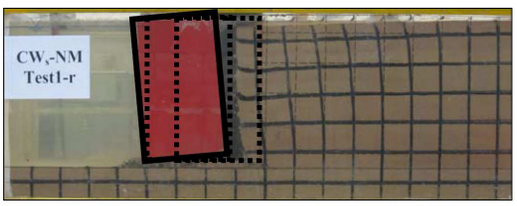

Figure 10. Measured post-earthquake deformed shape after the seismic loading

http://dx.doi.org/10.5772/55027

One might notice that the calculated results are rather close to measured values. This clearly demonstrates that the current numerical procedure captures very well the seismic behavior of the gravity-type quay wall and surrounding soils.

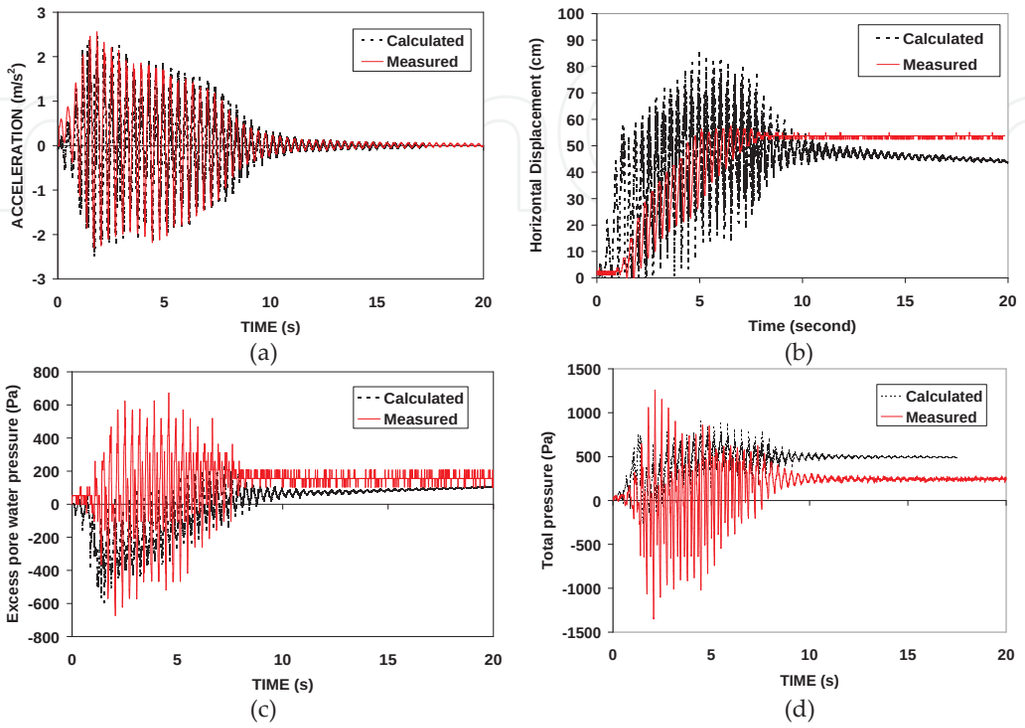

Figure 11. Recorded versus computed (a) acceleration, (b) horizontal displacement at top of the quay wall, and (c) excess pore water pressure, (d) total pressure behind the quay wall

4. Numerical results and discussion

Results of nonlinear effective-stress dynamic analyses are presented in this section to investigate the effects of soil properties and input excitation characteristics on liquefaction potential, deformation of quay wall and failure mechanisms of soil-wall system during seismic loading. For gravity quay walls on firm foundations, typical failure modes during earthquakes are seaward displacements and tilting. Therefore, the horizontal displacement of quay wall head is selected as a key parameter to judge about the stability of quay wall.

4.1. Influence of relative density of backfill soil

Three additional sets of soil properties with different relative densities are selected for backfill material (Dr = 15%, 25% and 40%). Figure 12(a) depicts the computed lateral displacement of the quay wall's head. The horizontal deformation for all relative densities is greater than allowable value proposed by PIANC (2001) and the quay wall system goes toward failure. After the earthquake, the system reaches to equilibrium. The final permanent deformations

and rate of increase for Dr=15% is much more than the others. Figure 12(b) shows cumulative vertical displacement (settlement) of the quay wall's head for the various backfill soil relative densities. As expected, the higher the relative density, the less the accumulated vertical permanent deformation. Figure 12(c) shows the excess pore water pressure ratio at far field in depth of 13 m for three different materials. It is clearly seen that the free field backfill is quickly liquefied. Figure 12(d) depicts the excess pore water pressure ratio time histories for various backfill soil relative densities behind the quay wall in depth of 13 m. It is found that the liquefaction does not occur in backfill soil behind the quay wall. This can be attributed to the movement of quay wall due to seismic loading which directly influences the pore pressure build up.

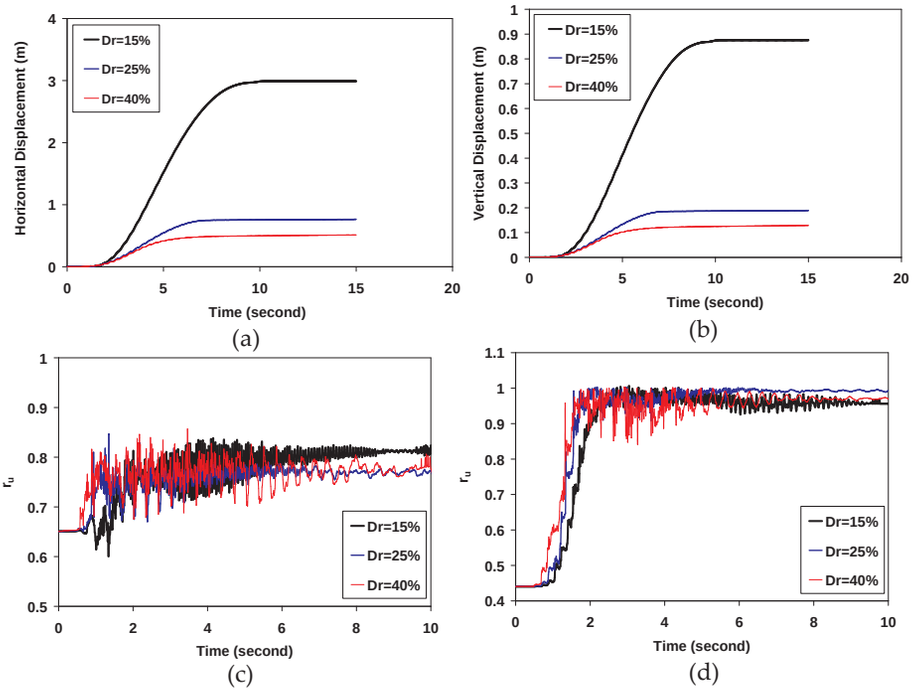

Figure 12. Computed values of: (a) horizontal deformation, and (b) vertical deformation of quay wall's head, and (c) excess pore water pressure ratio at far field, and (d) excess pore water pressure ratio behind the quay wall for various relative densities of backfill soil

Figure 13 shows the deformed shape after the seismic excitation for three sets of relative densities. As may be expected, more ground surface settlement is observed in the backfill near the wall than at the far field. One may observe that there is a significant movement of quay wall for Dr=15% rather than Dr=25% and 40%. Note also that the lateral spreading of soil is clearly visible near the area influenced by the quay wall especially for Dr=15%. In addition, differential settlements between the quay wall and the apron as well as the deformation of the foundation rubble beneath the quay wall are also observed in Figure 13. This is consistent with the common mode of deformation for gravity quay walls. The analysis indicates translation and rotation mode (rocking) of the wall.

http://dx.doi.org/10.5772/55027

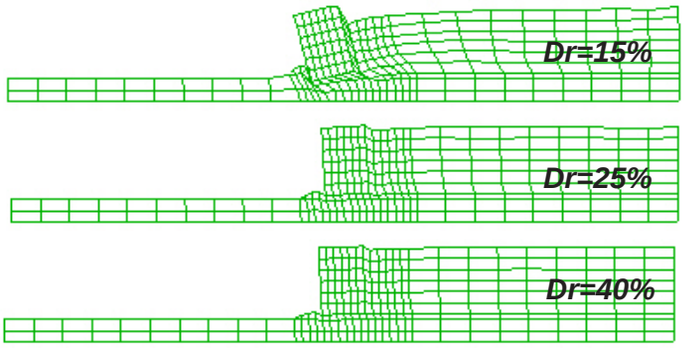

Figure 13. Deformed shape of the quay wall system for various relative densities of backfill soil

4.2. Influence of shear stiffness of backfill soil

Three different shear modulus values are adopted (G=20, 35 and 50 MPa) to investigate the effect of shear stiffness of the backfill soil. The other parameters are the same for all the analyses. Figures 14(a) and (b) show the permanent horizontal and vertical displacements time histories of the quay wall's head during seismic loading. It is observed that quay wall has significant movement toward the seaside. Both horizontal and vertical deformations are greater than the allowable limits which have been mentioned in PIANC (2001).

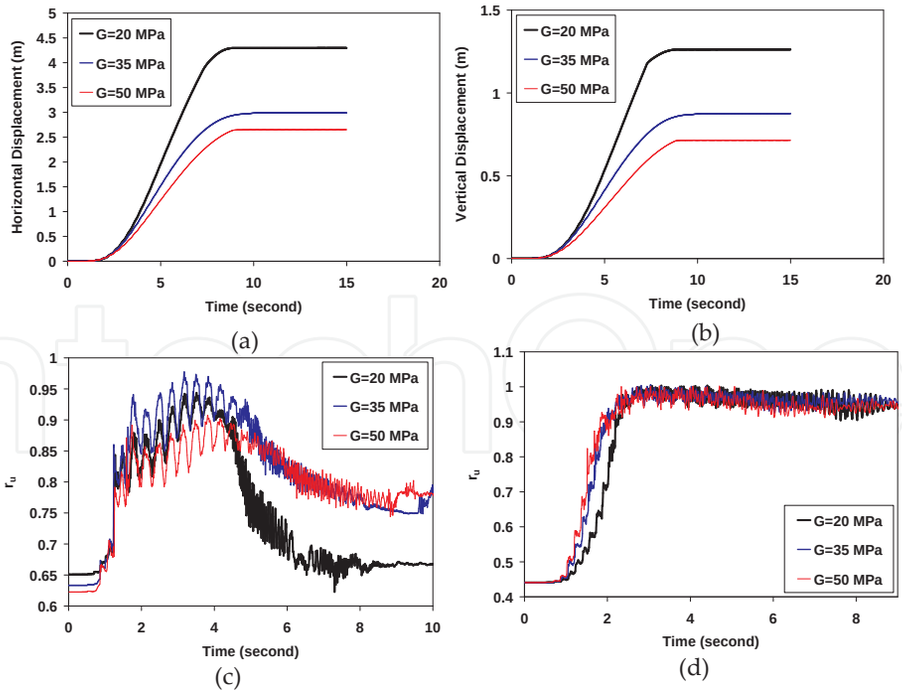

Figure 14. Computed values of: (a) horizontal deformation, and (b) vertical deformation of quay wall's head, and (c) excess pore water pressure ratio at far field, and (d) excess pore water pressure ratio behind the quay wall for various shear moduli of backfill soil

Figures 14(c) and (d) show the excess pore water pressure ratio time histories for the far field location and the area behind quay wall. The Figure 14(d) exhibits a significant increase in pore pressure which leads to liquefaction (r_u=1) for three types of backfill soil. But for the soil behind quay wall and adjacent to it, at first, the excess pore water pressure ratio increases quickly and after 4 seconds, the excess pore water pressure is dissipated rapidly and consequently, r_u decreases with time. This can be pertained to the quay wall movement during seismic loading which influences the excess pore water pressure. In addition, significant reduction is observed after 4.5 s for r_u at behind quay wall.

In Figure 15, lateral spreading is clearly obvious behind the quay wall for all the analyses. Deferential settlements between the quay wall and the apron are also visible. The major failure pattern is tilting and rotation of the quay wall toward the seaside which is consistent with the actual failure mode of quay wall movement in literature.

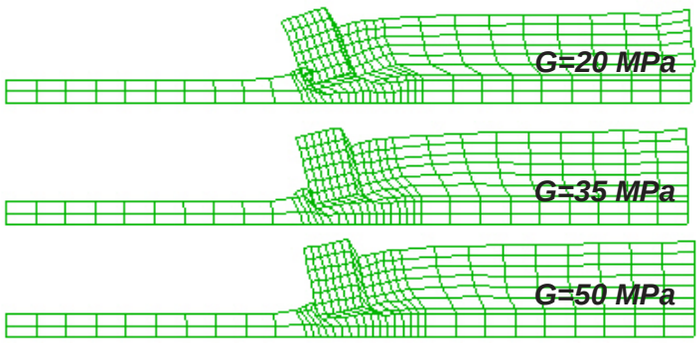

Figure 15. Deformed shape of the quay wall system for various shear moduli of backfill soil

4.3. Influence of friction angle of backfill soil

Figure 16(a) shows the calculated lateral deformation of quay wall's head for three different values of backfill soil friction angle (ϕ=25 , 30 *and* 35 degree). As may be expected, the higher the friction angle, the less the accumulated permanent deformation. The same trend as horizontal displacement is observed for the vertical displacement of quay wall's head. Both horizontal and vertical displacements generally increase with decreasing the friction angle of backfill soil.

Figures 16(c) and (d) show the time histories of excess pore water pressure ratio at the far field and the area behind quay wall, respectively. It is seen that the excess pore water pressure ratio at the far field reaches its maximum value (r_u=1) at around 2 s. At this time, liquefaction occurs. But for the region behind quay wall, liquefaction does not occur because the volume of backfill soil near the wall tends to increase during the outward movement of the wall. As previous results, Figure 17 demonstrates that the failure mode is rotation and the wall tends to rotate at the bottom.

http://dx.doi.org/10.5772/55027

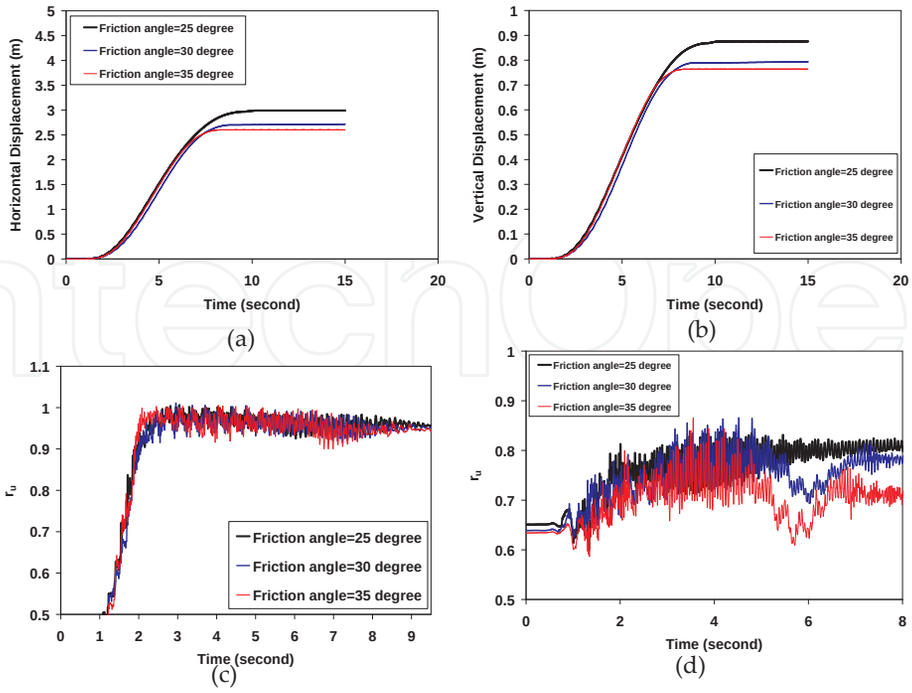

Figure 16. Computed values of: (a) horizontal deformation, and (b) vertical deformation of quay wall's head, (c) excess pore water pressure ratio at far field, and (d) excess pore water pressure ratio behind the quay wall for various friction angles of backfill soil

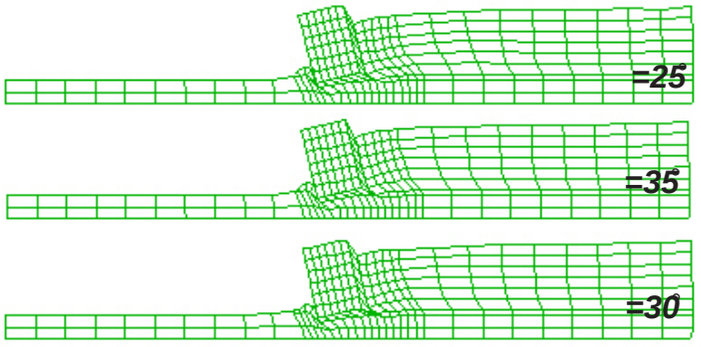

Figure 17. Deformed shape of the quay wall system for various friction angles of backfill soil

4.4. Influence of maximum amplitude of seismic loading

Three different maximum amplitudes are selected for the input excitation applied to the base of the model ($a_{\max}$=0.15g, 0.2g *and* .25g) to consider the effect of input excitation intensity. All other parameters are the same for all the analyses. Figures 18(a) and (b) show the horizontal and vertical displacements time histories at the top of quay wall subjected to seismic loading with different maximum amplitudes. As expected, by increasing the maximum amplitude of seismic loading, the deformation of quay wall increases, both laterally

and vertically. It is noticed that the values of displacements are much more than the allowable values recommended by PIANC (2001). It means that in such cases, the quay wall completely fails during loading.

Figures 18(c) and (d) depict r_u time histories at the far field and the area behind quay wall. As it is seen, the backfill soil liquefy at far field for all the maximum amplitude but at first liquefaction occurs for a_{max}=0.25g. For the area behind quay wall, r_u is less than 0.85 during seismic loading. Therefore, it can be concluded that liquefaction does not occur nearby (behind) the quay wall. The difference in pore pressure build up pattern between the far (free) field and near-wall field is mainly due to the fact that near the wall, soil experiences significant compression and extension alternatively during shaking (due to wall oscillation). In the free field, soil mainly experiences shear during shaking, allowing for high r_u and leading eventually to liquefaction.

Figure 19 indicates translation and rotation (rocking) of the quay wall. Lateral spreading and ground failure behind the quay wall are clearly observed. As may be expected, more ground surface settlement is noticed in the backfill near the wall than at the far field. A large tilting of the wall to the seaward is obviously observed.

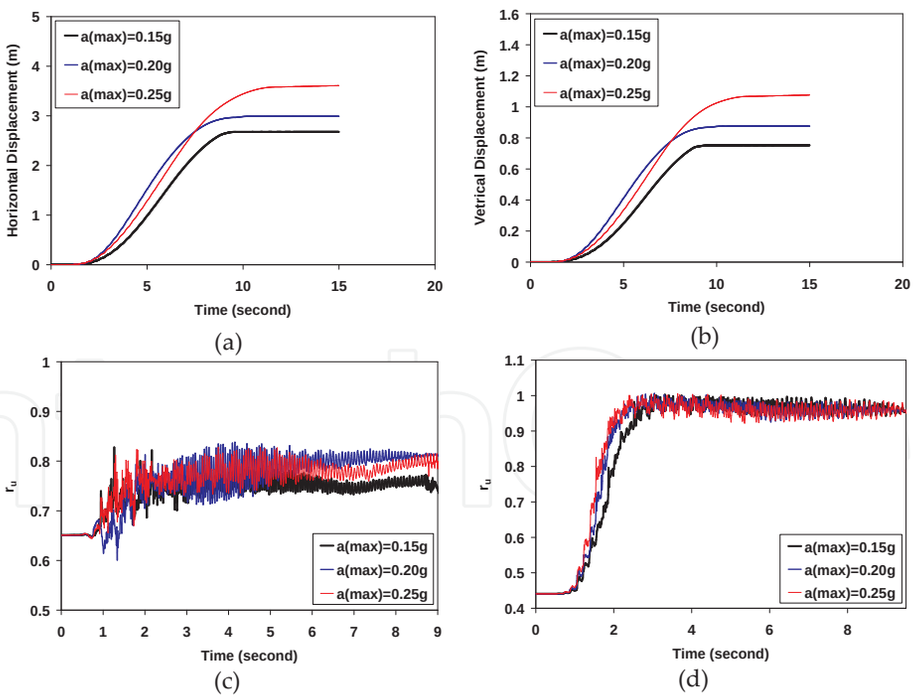

Figure 18. Computed values of: (a) horizontal deformation, and (b) vertical deformation of quay wall's head, (c) excess pore water pressure ratio at far field, and (d) excess pore water pressure ratio behind the quay wall for various maximum amplitudes of the seismic loading

http://dx.doi.org/10.5772/55027

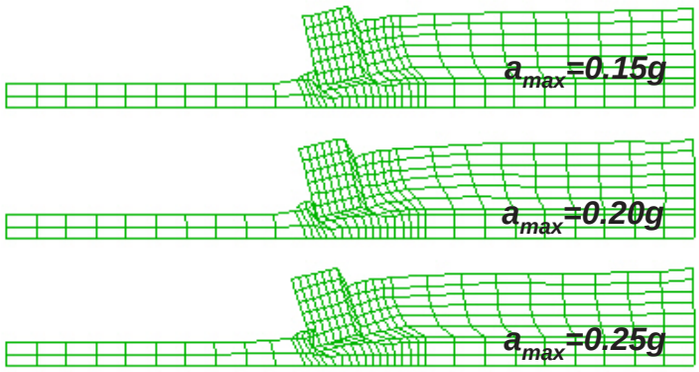

Figure 19. Deformed shape of the quay wall system for various maximum amplitudes of the seismic loading

4.5. Influence of frequency of seismic loading

Figures 20(a) and (b) indicate the horizontal and vertical displacements time histories of the quay wall's head during seismic loading. As may be expected, by increasing the frequency of seismic loading, the displacements increase excessively and the quay wall system entirely fails. The values of displacements are so much higher than allowable values proposed by PIANC (2001).

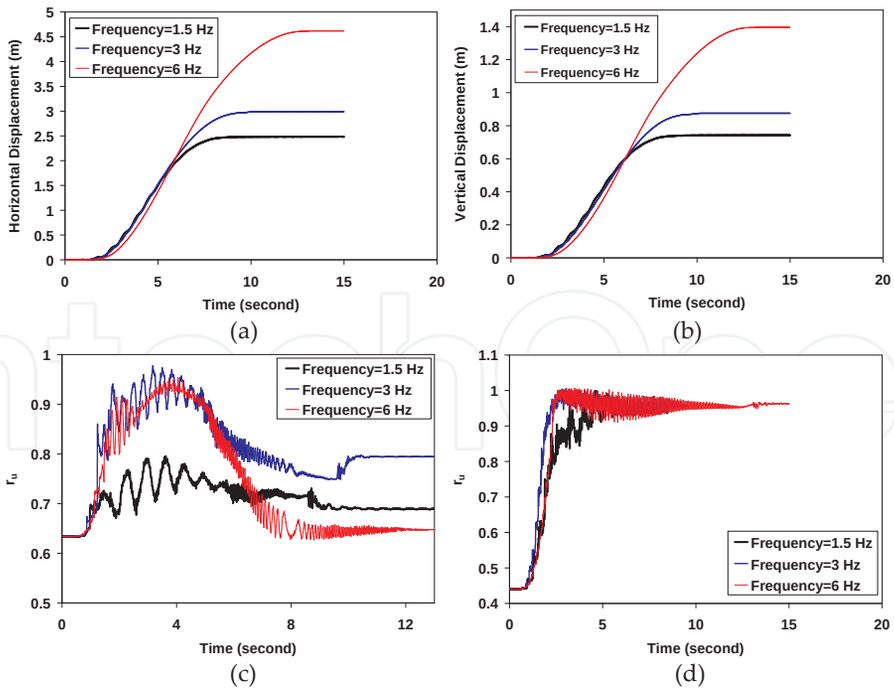

Figure 20. Computed values of: (a) horizontal deformation, and (b) vertical deformation of quay wall's head, and (c) excess pore water pressure ratio at far field, and (d) excess pore water pressure ratio behind the quay wall for various frequencies of the seismic loading

As pervious, liquefaction occurs at the far field which is not affected by the quay wall movement (Figure 20(c)) but for the area behind quay wall, liquefaction does not occur due to seaward movement of the quay wall (Figure 20(c)). As it is clear in Figure 20(d) that the excess pore pressure ratio increases till 4 seconds but after that dissipation is observed for all frequencies. The rate of dissipation for frequency of 6 Hz is higher than the others. Figure 21 depicts the deformed shape of quay wall system after seismic loading. As it is seen, the lateral spreading behind quay wall completely observed for all frequencies but it is much more severe for F=6 Hz which the quay wall has been failed entirely and the area behind quay wall has subsided excessively. The failure mode of the quay wall is translation and rotation. When the frequency of seismic loading increases, the quay wall rotates more.

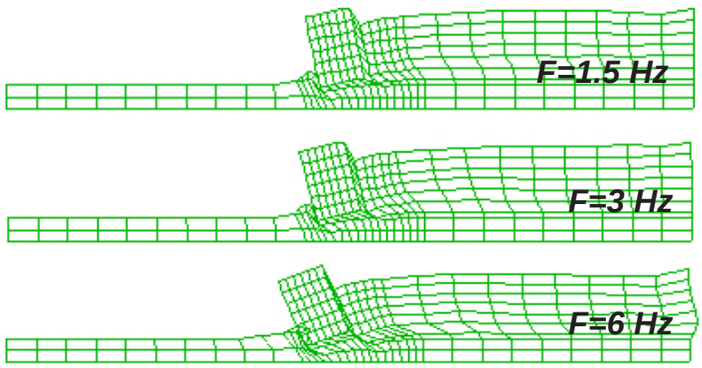

Figure 21. Deformed shape of the quay wall system for various frequencies of the seismic loading

5. Conclusions

In this study, 2D nonlinear effective stress dynamic analyses have been carried out to investigate the seismic behavior of gravity-type quay walls. A reference model has been constructed and then subjected to seismic loading. The Finn and Byrne model has been adopted with some slightly modifications which take into account the pore water pressure generation and liquefaction process under dynamic loading. The numerical model has been validated by simulating 1g shaking table test. It is shown that the obtained numerical results agree reasonably with actual observation in the shaking table test. The seismic response of the gravity wall itself has well captured by the numerical analyses with satisfactory predictions of acceleration, displacement, total pressure and pore water pressure time histories. Additional computational parametric studies have been conducted by varying backfill soil relative density, shear modulus, friction angle and maximum amplitude and frequency of input excitation to study the extent of liquefaction and deformation mechanism of quay wall system. It is concluded that soil properties and input motion characteristics are among the most influential factors in dictating seismic performance of the quay wall system. The results show that the backfill in the soil-wall interaction zone and the foundation soils beneath the quay wall experiences less excess pore water pressure even liquefaction occurs in the far field during shaking. The

http://dx.doi.org/10.5772/55027

alternative pumping and suction process in excess pore water pressure which are caused by wall's vibrations increase the level of damage because large amounts of backfill are forcedly leaked into the sea. The lack of backfill liquefaction near the wall is attributed to the lateral displacement of the wall. In the other words, excess pore water pressure does not attain 100% liquefaction behind the quay wall contrary to the far field. The current study states that the numerical simulation incorporated with the special numerical techniques is capable of modeling the seismic response of gravity-type quay walls.

Author details

Babak Ebrahimian*

School of Civil Engineering, Faculty of Engineering, University of Tehran, Tehran, Iran

References

[1] Arulanandan, K. (1996). Application of numerical procedures in geotechnical earthquake engineering, *Proceeding of Application of Numerical Procedures in Geotechnical Earthquake Engineering*, National Science Foundation Workshop/ Conference, October 28-30.

[2] American Society of Civil Engineers, (2000). ASCE 4-98 Seismic Analysis of Safety-related Nuclear Structures and Commentary. *ASCE*, Virginia, USA.

[3] Byrne, P. M. (1991). A cyclic shear-volume coupling and pore pressure model for sand, *Proceeding of Second International Conference on Recent Advances in Geotechnical Earthquake Engineering and Soil Dynamics*, Vol. 1, University of Missouri, Rolla, Missouri, pp. 47-55.

[4] Chen, C., Hwang, G. (1969). Preliminary analysis for quay wall movement in Taichung harbour during the September 21, 1999, Chi-Chi earthquake, *Earthquake Engineering and Engineering Seismology*, Vol. 2, pp. 43-54.

[5] Cooke, H. G. (2000). Ground improvement for liquefaction mitigation at existing highway bridges, *Ph.D. dissertation*, Department of Civil and Environmental Engineering, Polytechnic Institute and State University, Virginia.

[6] Dickenson, S. E., Yang, D. S. (1998). Seismically-induced deformations of caisson retaining walls in improved soils, *Proceeding of Geotechnical Earthquake Engineering and Soil Dynamics III, Vol. II, Geotech. Special Pub*. No. 75., ASCE, Reston, VA, pp. 1071-1082.

[7] Ebrahimian, B., Mostafavi Moghadam, A. A., Ghalandarzadeh, A. (2009). Numerical modeling of the seismic behavior of gravity type quay walls, *Proceeding of Perform-*

ance-based Design in Earthquake Geotechnical Engineering—Kokusho, Tsukamoto , Yoshimine (eds), Taylor & Francis Group, London, ISBN 978-0-415-55614-9, Tokyo, June 15–18.

[8] Finn, W.D.L., Lee, K.W., Martin, G.R. (1977). An effective stress model for liquefaction. *Journal of Geotechnical Engineering Division ASCE*, Vol. 103, No. 6, pp. 517-553.

[9] Finn, W. D. L. (1988). Dynamic analysis in geotechnical engineering, *Proceeding of Earthquake Engineering and Soil Dynamics II - Recent Advances in Ground Motion Evaluation*, ASCE Geotechnical Engineering Division,Park City, Utah, June, pp. 523-591.

[10] Finn, W. D. L. (1991). Estimating how embankment dams behave during earthquakes, *Water Power and Dam Construction,* London, April, pp. 17-22.

[11] Hayashi, S., Kubo, K., Nakase, A. (1966). Damage to harbour structures by the Nigata earthquake, *Journal of Soils and Foundations,* Vol. 6, No. 1, pp. 89-111.

[12] Iai, S. (1998). Seismic analysis and performance of retaining structures, *Proceedings of the 1998 Conference on Geotechnical Earthquake Engineering and Soil Dynamics III*, Part 2 (of 2), ASCE, pp. 1020-1044.

[13] Iai, S., Ichii, K., Liu, H., Morita, T. (1998). Effective stress analysis of port structures, *Special issue of soils and foundations,* pp. 97-114.

[14] Iai, S., Sugano, T. (2000). Shaking table testing on seismic performance of gravity quay walls, *12 WCEE*.

[15] Ichii, K., Iai, S., Morita, T. (2000). Performance of the quay wall with high seismic resistance, *Journal of Computing in Civil Engineering*, Vol. 17, No. 2, pp. 163-174.

[16] Inagaki, H., Iai, S., Sugano, T., Yamazaki, H., Inatomi, T. (1996). Performance of cassion type quay walls at Kope Port, *Special issue of soils and foundations*, pp. 119-136.

[17] Inoue, K., Miura, K., Otsuka, N., Yoshida, N., Sasajima, T. (2003). Numerical analysis of the earth pressure during earthquake on the gravity type quay wall, *Proceedings of the Thirteenth (2003) International Offshore and Polar Engineering Conference*, International Society of Offshore and Polar Engineers, Honolulu, United States., pp. 2095-2099.

[18] Itasca, (2004). FLAC User's Guide, Version 4.0, *Itasca Consulting Group. Inc,* Minnesota, USA.

[19] Kuhlemeyer, R.L., Lysmer, J. (1973). Finite element method accuracy for wave propagation problems, *Journal of Soil Mechanics and Foundations ASCE,* Vol. 99, No. SM4, pp. 421-427.

[20] Lysmer, J., Kuhlmeyer, R.L. (1969). Finite element method for infinite media, *Journal of Engineering Mechanics ASCE*, Vol. 95, No. EM4, pp. 859-877.

[21] Madabhushi, S. P. G., Zeng, X. (1998). Seismic response of gravity quay walls. II: numerical modeling, *Journal of Geotechnical and Geoenvironmental Engineering ASCE*, Vol. 124, No. 5, pp. 418-427.

[22] Martin, G. R., Finn, W. D. L., Seed, H. B. (1975). Fundamentals of liquefaction under cyclic loading, *Journal of Geotechnical Division ASCE*, Vol. 101(GT5), pp. 423-438.

[23] Masing, G. (1926). Eigenspannungen und Verfestigung Beim Messing, *Proceedings of 2nd International Congress on Applied Mechanics*, Zurich.

[24] McCullough, N. J., Dickenson, S. E. (1998). Estimation of seismically induced lateral deformations for anchored sheetpile bulkheads. *Proceeding of Geotechnical Earthquake Engineering and Soil Dynamics III,* Seattle, USA.

[25] Mostafavi Moghadam, A. A., Ghalandarzadeh, A., Towhata, I., Moradi, M., Ebrahimian, B., Haji Alikhani, P. (2009). Studying the effects of deformable panels on seismic displacement of gravity quay walls, *Ocean Engineering*, Vol. 36, pp. 1129–1148.

[26] Mostafavi Moghadam, A. A., Ghalandarzadeh, A., Moradi, M., Towhata, I., Haji Alikhani, P. (2011). Displacement reducer fuses for improving seismic performance of caisson quay walls, *Bulletin of Earthquake Engineering*, Vol. 9, pp. 1259–1288.

[27] Nozu, A., Ichii, K., Sugano, T. (2004). Seismic design of port structures, *Journal of Japan association for earthquake engineering*, Vol. 4, pp. 195-208.

[28] Parra, E. (1996). Numerical modeling of liquefaction and lateral ground deformation including cyclic mobility and dilation response in soil systems, *Ph.D. Dissertation*, Department of Civil Engineering, RPI, Troy, NY.

[29] PIANC, 2001. Seismic Design Guidelines for Port Structures, A.A. Balkema, Rotterdam.

[30] Pyke, R. (1979). Nonlinear soil models for irregular cyclic loadings, *Journal of Geotechnical Division ASCE*, Vol. 105(GT6), pp. 715-726.

[31] Sasajima, T., Sakikawa, M., Miura, K., Otsuka, N. (2003). In-situ observation system for seismic behavior of gravity type quay wall, *Proceedings of the Thirteenth (2003) International Offshore and Polar Engineering Conference*, International Society of Offshore and Polar Engineers, Honolulu, United States, pp. 2087-209.

[32] Seed, H. B., Idriss, I. M. (1970). Soil moduli and damping factores for dynamic response analyses, *Report EERC 70-10, Earthquake Engineering Research Center*, University of California, Berkeley, CA.

[33] Seed, H. B., DeAlba, P. (1986). Use of SPT and CPT tests for evaluating the liquefaction resistance of soils, *Proceedings of Insitu 1986, ASCE*.

[34] Sugano, T., Morita, T., Mito, M., Sasaki, T., Inagaki, H. (1996). Case studies of cassion type quay wall damage by 1995 Hyogoken-Nanbu eartjquake, *Eleventh world conference on earthquake engineering*, Elsevier Science Ltd.

[35] Sumer, B.M., Kaya, A., Hansen, N. E. O. (2002). Impact of liquefaction on coastal structures in the 1999 Kocaeli, Turkey earthquake, *Proceedings of the Twelfth (2002) International Offshore and Polar Engineering Conference*, International Society of Offshore and Polar Engineers, Kitakyushu, Japan, 12, pp. 504-511.

[36] Westergaard, H. (1931). Water pressure on dams during earthquakes, *Transactions of ASCE*, pp. 418-433.

[37] Yang, Z. (2000). Numerical modeling of earthquake site response including dilation and liquefaction, *Ph.D. Dissertation*, Department Of Civil Engineering and Engineering Mechanics, Columbia University, New York, NY